Chimeras on annuli

Carlo R. Laing[a)]

(Dated: 18 July 2022)

Chimeras occur in networks of coupled oscillators and are characterised by the coexistence of synchronous and asynchronous groups of oscillators in different parts of the network. We consider a network of nonlocally coupled phase oscillators on an annular domain. The Ott/Antonsen ansatz is used to derive a continuum level description of the oscillators' expected dynamics, in terms of a complex-valued order parameter. The equations for this order parameter are numerically analysed in order to investigate solutions with the same symmetry as the domain, and chimeras which are analogous to the "multi-headed" chimeras observed on one-dimensional domains. Such solutions are stable only for domains with widths that are neither too large nor too small. We also study rotating waves with different winding numbers which are similar to spiral wave chimeras seen in two dimensional domains. We determine ranges of parameters such as the size of the domain for which such solutions exist and are stable, and the bifurcations by which they lose stability. All of these bifurcations appear subcritical.

Chimeras are novel spatiotemporal patterns which occur in networks of oscillators, characterised by coexisting regions of synchronised and asynchronous oscillators. While they have been studied on one-, two- and three-dimensional domains, here we consider an annular domain. We find solutions analogous to the "multi-headed" chimeras observed on ring networks, and rotating waves with varying levels of synchrony in the radial direction. We numerically analyse these patterns in the continuum limit, using the Ott/Antonsen ansatz to derive an exact description of the oscillators' expected state. Numerical bifurcation theory is used to determine the regions of existence and stability of a variety of chimera-like patterns.

I. INTRODUCTION

The study of synchronisation in networks of oscillators is a topic of much interest[46,50]. One phenomenon of recent prominence is the existence of chimeras — states characterised by the coexistence of synchronous and asynchronous groups of oscillators[31,42]. These have been studied in networks that can be thought of as having zero[2,23,44,45,47], one[4,15,52,53], two[30,37,43,49,54] or three[26–28] spatial dimensions. In two spatial dimensions, the domains considered include the surface of a sphere[22,43] a "flat" torus, i.e. a square domain with periodic boundary conditions[14,37,41,54], and a square domain with boundary conditions which take into account the lack of oscillators outside the domain[18]. The coupling between oscillators is normally nonlocal, although chimeras can exist when coupling is only local[20]. The existence of chimeras was first studied using self-consistency arguments[3,15,30], and later the Ott/Antonsen ansatz[38,39] was used to determine their stability[18]. However, this theory is only applicable to sinusoidally coupled phase oscillators, and many recent results relate to only numerical simulation of networks of oscillators[55].

[a)]School of Mathematical and Computational Sciences, Massey University, Private Bag 102-904 North Shore Mail Centre, Auckland, New Zealand. c.r.laing@massey.ac.nz

Here we consider spatiotemporal patterns on annular domains, using the Kuramoto model of sinusoidally coupled phase oscillators[5,16]. We consider nonlocally coupled heterogeneous oscillators with frequencies randomly chosen from a Lorentzian distribution in order to use the Ott/Antonsen ansatz[38,39] to derive continuum level equations whose fixed points and bifurcations thereof can be studied numerically. An annulus has two limiting cases for which we can compare our results to previous work: the inner radius is zero, corresponding to a circular domain[30], and equal inner and outer radii, corresponding to a ring[4,18].

The continuum version of nonlocally coupled phase oscillators in two spatial dimensions can be written[22,43]

$$\frac{\partial\theta(\mathbf{x})}{\partial t}=\omega(\mathbf{x})-\int W(|\mathbf{x}-\mathbf{x}'|^2)\sin[\theta(\mathbf{x})-\theta(\mathbf{x}')+\alpha]d\mathbf{x}' \tag{1}$$

where $\theta(\mathbf{x})$ and $\omega(\mathbf{x})$ are the phase and intrinsic frequency, respectively, of the oscillator at position $\mathbf{x}$ and the integral is taken over the domain. The nonlocal coupling is described by the function W, which we write as a function of distance squared. We will use

$$W(r)=e^{-r}, \tag{2}$$

corresponding to a Gaussian kernel.

Writing the polar coordinates of $\mathbf{x}$ as (r,ϕ) and those of $\mathbf{x}'$ as $(s,\phi+\psi)$ we find that $|\mathbf{x}-\mathbf{x}'|^2=r^2+s^2-2rs\cos\psi$ and thus on an annular domain we have

$$\frac{\partial\theta(r,\phi)}{\partial t}=\omega(r,\phi)$$
$$-\int_a^b s\int_{-\pi}^{\pi}W(r^2+s^2-2rs\cos\psi)\sin[\theta(r,\phi)-\theta(s,\phi+\psi)+\alpha]\,d\psi\,ds \tag{3}$$

where a and b are the inner and outer radii of the domain, respectively, and for simplicity we do not show time dependence explicitly. The heterogeneity is introduced by choosing the value of ω at each point in the domain from a Lorentzian with mean zero and width δ. In practice, when numerically solving (3) we discretise both the radial and angular directions with regular grids.

Using a standard derivation[22,53] we can use the Ott/Antonsen ansatz to derive the corresponding evolution equation for the complex-valued order parameter z:

$$\frac{\partial z(r,\phi)}{\partial t} = -\delta z + e^{-i\alpha}R/2 - e^{i\alpha}\bar{R}z^2/2 \tag{4}$$

where

$$R(r,\phi) = \int_a^b s \int_{-\pi}^{\pi} W(r^2+s^2-2rs\cos\psi) z(s,\phi+\psi)\, d\psi\, ds \tag{5}$$

and overbar indicates the complex conjugate.

The physical interpretation of $z(r,\phi)$ is that the distribution of phases, θ, at (r,ϕ) is

$$P(\theta) = \frac{1-|z|^2}{2\pi\left[1-2|z|\cos(\theta-\arg z)+|z|^2\right]}, \tag{6}$$

a unimodal function of θ with a peak at $\theta = \arg z$, whose sharpness depends on $|z|$: $|z|=0$ corresponds to a uniform distribution while as $|z|\to 1$ the distribution approaches a Dirac delta function at $\theta = \arg z$[18,36].

More generally, one can treat (4)-(5) as a dynamical system in itself. For fixed (r,ϕ), (4) is a complex Riccati equation[32,33]. We can also regard $z(r,\phi)$ as the state of a planar "oscillator" at (r,ϕ) with amplitude $|z|$ and phase $\arg(z)$, where $|z|$ encodes the level of local synchrony at (r,ϕ). Thus (4) is similar in form to a Stuart-Landau oscillator, and with coupling (5), to a nonlocally coupled complex Ginzburg–Landau equation[12].

Note that (4)-(5) is invariant under the transformation $z \to ze^{i\gamma}$ for any γ, which suggests moving to a rotating coordinate system. In this rotating coordinate system (4) is replaced by

$$\frac{\partial z(r,\phi)}{\partial t} = (i\Omega-\delta)z + e^{-i\alpha}R/2 - e^{i\alpha}\bar{R}z^2/2 \tag{7}$$

where Ω is the speed of rotation of the coordinate frame. The solutions we are interested in are fixed points of (7) where $R(r,\phi)$ is given by (5), and the rest of the paper concerns the solutions of these two equations.

The work most similar to ours is[10], who consider nonlocally coupled *identical* phase oscillators on an annulus. These authors make more analytical progress than we can, as the state of each oscillator is described by a single angular variable, whereas using the Ott/Antonsen ansatz, the *expected* state of each oscillator — described by a probability density function parametrised by a complex variable z with both a magnitude and a phase — is the quantity of interest. An advantage of the approach here is that we can describe varying levels of synchrony (chimeras), and the equations do not break down when a single oscillator breaks away, as occurs in the description used in[10]. Another difference between our work and that in[10] is that they considered an interaction function (the $\sin(\cdot)$ in (3)) which is zero if the phases at two different points in the domain are the same. This means that complete synchrony is always a solution. However, having a nonzero phase offset α in (3), as we do, is likely to promote the existence of chimeras[30]. And it is well-known that varying α is likely to cause a chimera to undergo a bifurcation[2,18]. Choosing heterogeneous oscillators of the form used here means that the Ott/Antonsen manifold (corresponding to solutions derived using the Ott/Antonsen ansatz) is stable, and thus we can determine the asymptotic dynamics by restricting to this manifold. If the oscillators were identical one could still use the Ott/Antonsen ansatz, but a more complete description would require use of the Watanabe/Strogatz ansatz[51]. However, the equations resulting from the latter ansatz are known to have continuous families of neutrally stable solutions which are difficult to study numerically, unlike those derived with the Ott/Antonsen ansatz.

The structure of the paper is as follows. In Sec II we study solutions which are invariant under rotation about the centre of the annulus (rotationally symmetric solutions). In Sec. III we consider the analogue of the "one-headed" or classical chimera on a ring. We then move on to "multi-headed" chimeras in Sec. IV. The other form of chimera that can occur on an annulus is a rotating wave or spiral wave chimera, and these are considered in Sec. V. The stability of the zero solution, corresponding to complete asynchrony, is examined in Sec. VI and we conclude in Sec. VII.

II. ROTATIONALLY SYMMETRIC SOLUTIONS

A rotationally symmetric solution of (7) has no dependence on ϕ, and is governed by

$$\frac{\partial z(r)}{\partial t} = (i\Omega-\delta)z + e^{-i\alpha}R/2 - e^{i\alpha}\bar{R}z^2/2 \tag{8}$$

where

$$R(r) = \int_a^b s \int_{-\pi}^{\pi} W(r^2+s^2-2rs\cos\psi) z(s)\, d\psi\, ds. \tag{9}$$

Using the Gaussian (2) we have

$$R(r) = e^{-r^2}\int_a^b s e^{-s^2} z(s) \int_{-\pi}^{\pi} e^{2rs\cos\psi}\, d\psi\, ds.$$

But

$$\int_{-\pi}^{\pi} e^{2rs\cos\psi}\, d\psi = 2\pi I_0(2rs)$$

where I_0 is the modified Bessel function of the first kind, so

$$R(r) = 2\pi e^{-r^2}\int_a^b I_0(2rs) s e^{-s^2} z(s)\, ds \tag{10}$$

Rotationally symmetric solutions are thus described by the one-dimensional integro-differential equation (8) with (10). Clearly $z=0$ is a fixed point of these equations, but we are interested for now in nontrivial solutions. Note that (8) and (10) are invariant under the transformation $z \to ze^{i\gamma}$ for any γ, so to remove this invariance (and determine Ω) we need to append a "pinning" condition such as $\arg(z(a)) = 0$ which selects one solution from this continuous family when finding steady states.

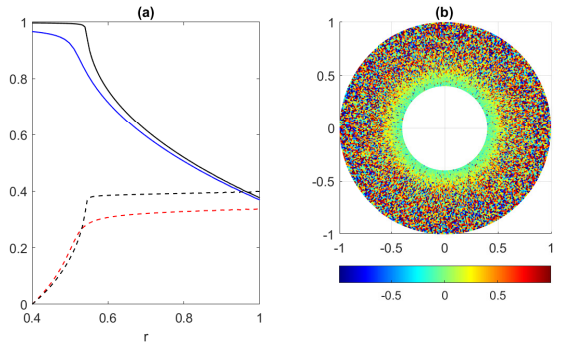

FIG. 1. A example of a rotationally symmetric solution for which z is independent of the angular position in the domain. (a) Stable steady state of (8) for $\delta = 0.01$. Blue solid: $|z|$; red dashed: $\arg(z)$. The black curves show the same quantities (matching line styles) for $\delta = 0.001$. (b) Snapshot of $\sin\theta$ for the discrete system (3) with $\delta = 0.01$. Other parameters: $a = 0.4, b = 1, \alpha = \pi/2 - 0.08$.

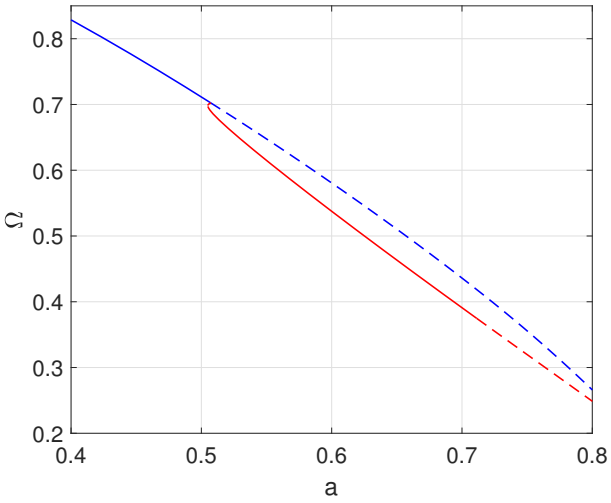

FIG. 2. Existence and stability of rotationally symmetric and "1-head" chimera solutions. Ω as a function of a for a rotationally symmetric solution (blue) and "1-head" chimera (red). Solid: stable, dashed: unstable. Other parameters: $b = 1, \delta = 0.01, \alpha = \pi/2 - 0.08$. There is a small range of a values, just above $a = 0.5$, for which both solutions are stable. The rightmost instability of the 1-head solution is a subcritical Hopf bifurcation.

A. Results

We fix parameters $\delta = 0.01, \alpha = \pi/2 - 0.08$. The integral in (10) is approximated using the trapezoidal rule. A typical stable steady state of (8) shown in Fig. 1(a), in colour. The nonzero value of δ means that oscillators can never perfectly lock, so $|z| < 1$. We see that oscillators near the inner boundary are nearly synchronous ($|z| \approx 1$), and they become less synchronous ($|z|$ decreases) as we move towards the outer radius. Note that we have shifted the argument of z so that it is zero at the inner radius. Panel (b) shows a snapshot of $\sin\theta$ for the discrete network (3). As δ is decreased the distinction between synchronous and asynchronous oscillators becomes clearer, as shown by the black curves in panel (a) corresponding to $\delta = 0.001$.

There is no universally accepted definition of a chimera[13], but we argue that despite differing levels of synchrony within the domain, the solution shown is not a chimera, in the same way that the partially synchronous solution of the Kuramoto model[5] is not a chimera. The different levels of synchrony are a result of the shape of the domain and the differing levels of influence that other oscillators have on a specific one: those near the inner radius receive a different (weighted) input than those near the outer radius. In addition, this solution has the same symmetry as the domain, i.e. that of a circle, whereas chimeras are generally thought of as resulting from the breaking of some symmetry of the domain.

We are interested in bifurcations caused by changing the geometry of the domain, and following this rotationally symmetric solution as a is increased we obtain Fig. 2. The solution undergoes a subcritical symmetry-breaking bifurcation producing an unstable "1-head" chimera which we analyse in the next section. The rotationally symmetric solution remains stable as a is decreased to zero. (Stability is determined by linearising the full dynamics (7) about the rotationally symmetric solution.) The largely coherent region remains localised near the inner boundary and at $a = 0$ we obtain a stable coherent spot solution, as seen in[22,37] (not shown).

III. ONE-HEAD CHIMERA

The term "multi-headed" chimera refers to chimeras on a one-dimensional domain for which there are multiple incoherent regions ("heads") alternating with coherent regions[29]. Thus the classical chimera on a ring[4,15] could be referred to as a "one-head" chimera. For a thin annulus (with similar inner and outer radii) we expect to see a similar state for some parameter values. An example of such a solution is shown in Fig. 3. In panel (a) we see $|z|$ for a steady state of (7). There is a spatially-localised region of almost synchronous oscillators (where $|z|$ is near 1) near the inner radius while the rest of the domain is largely asynchronous. A snapshot of a solution to (3) is shown in Fig. 3 (b). The position of the synchronous group is largely determined by the initial conditions, and thus they do not match in the two panels. This solution is a chimera, as it has less symmetry than that of the domain. There is a continuum of such solutions, parametrised by their angular position in the domain, just as for the classical chimera on a ring[4,15]. Also, the average frequency of the largely synchronous oscillators is different from that of the asynchronous ones (not shown), as required. As above, decreasing δ makes it more clear that this solution consists of a small region of nearly synchronous oscillators with the remainder being largely asynchronous (not shown).

Following this one-head chimera as a is varied we obtain the red curve in Fig. 2. As mentioned, it is created in a subcritical symmetry-breaking bifurcation from the rotationally symmetric solution when a is slightly larger than 0.5. It quickly

becomes stable through a saddle-node bifurcation and then as a is increased it loses stability through a Hopf bifurcation which (from numerical simulations) appears to be subcritical.

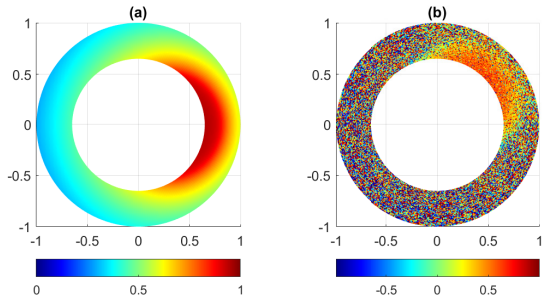

FIG. 3. Two representations of a "1-head" chimera. (a): $|z|$ for a steady state of (7). ($|z|$ close to 1 indicates approximate synchrony.) (b): a snapshot of $\sin\theta$ for (3). Parameters: $a = 0.65, b = 1, \delta = 0.01, \alpha = \pi/2 - 0.08$.

IV. MULTI-HEADED CHIMERAS

On a ring network, multi-headed chimeras with even numbers of heads have been observed[29]. On an annular domain we also see two-headed, four-headed and six-headed chimeras, as shown in Fig. 4. The left column shows $|z|$, and we clearly see the alternating regions of high and low synchrony. The phases of successive highly-synchronous groups differ by π, as seen from the right column, where $\arg(z)$ is plotted. (Note that a constant can be added to the phase of z at a steady state of (4), and we have chosen this constant to make clear this phase difference.) These states are all stable, and initial conditions similar to the solutions of interest must be used in order to find them. Solutions with more heads can be found for domains with larger circumferences.

To uncover bifurcations due purely to varying the geometry of the domain we keep b constant and vary a, as done for Fig. 2. The results for the two-head chimera are shown in Fig. 5. The solution loses stability at $a = 1.15$ and at $a = 0.53$. Both of these bifurcations are Hopf bifurcations, and from numerically solving (4) it seems that both bifurcations are subcritical. Also shown in Fig. 5 is an example of an unstable two-head chimera. Stability was determined by linearising (7) about the corresponding steady state.

Varying a the four-head chimera loses stability at $a = 2.19$ and at $a = 1.48$ as shown in Fig. 6. Both of these are symmetry-breaking bifurcations, and from numerically solving (4) it seems that both bifurcations are subcritical. Also shown in Fig. 6 is an example of an unstable four-head chimera.

Varying a the six-head chimera loses stability at $a = 1.46$ in a subcritical Hopf bifurcation and at $a = 1.87$ in a subcritical symmetry breaking bifurcation, as shown in Fig. 7. Also shown in Fig. 7 is an example of an unstable six-head chimera.

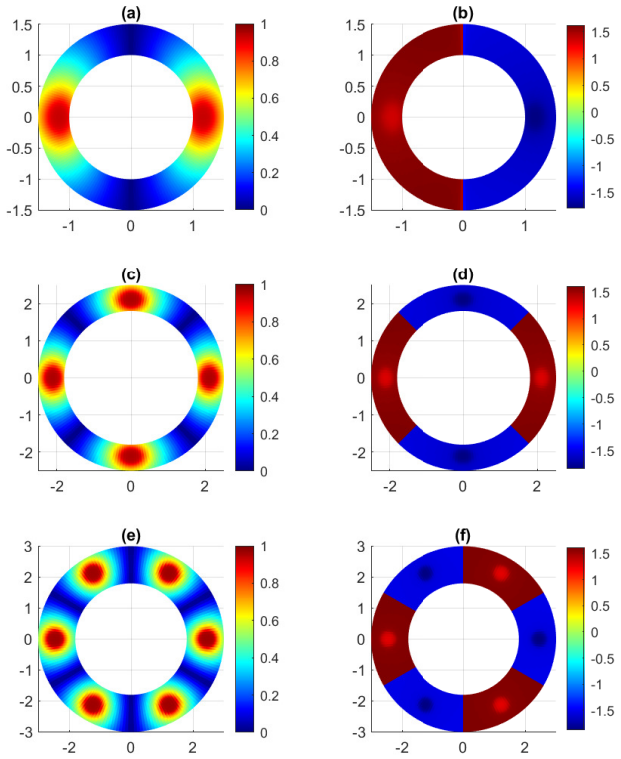

FIG. 4. Examples of stable multi-headed chimera solutions of (7). (a) and (b): a two-headed chimera; (c) and (d): a four-headed chimera; (e) and (f): a six-headed chimera. The left column shows $|z|$, indicating the level of local synchrony, and the right shows $\arg(z)$. Parameters: $\delta = 0.01, \alpha = \pi/2 - 0.08$. 2-head: $(a,b) = (1, 1.5)$, 4-head: $(a,b) = (1.8, 2.5)$, 6-head: $(a,b) = (1.8, 3)$.

In summary, we have found multi-headed chimeras on annular domains which are analogous to those found on ring domains[29]. They occur for α slightly smaller than $\pi/2$, the same range in which other chimeras of this form have been found[3,31]. Holding the outer radius b and the parameter α constant while varying the inner radius a, we find that these solutions exist all the way down to $a = 0$ (i.e. a circular domain) but are stable only for a range of values of a bounded away from both 0 and b. These solutions all seem to undergo subcritical bifurcations as a is varied, past which the system jumps to a very different type of solution. All of the stable chimeras shown here have been reproduced in simulations of the discrete network (3) (not shown). Regarding the loss of stability as $a \to b$, note that $R \to 0$ in this limit, so to obtain the correct equation describing oscillators on a ring (and to not have $\Omega \to 0$) in this limit one could alternatively consider a model in which R is normalised by the area of the annulus, i.e. R is replaced by $R/[\pi(b^2 - a^2)]$.

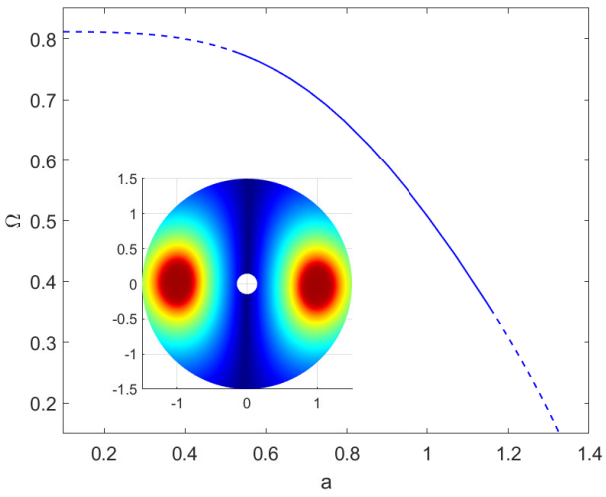

FIG. 5. Existence and stability of a two-head chimera. Ω is plotted as a function of a for the two-head chimera. Solid: stable; dashed: unstable. The inset shows $|z|$ for the unstable solution at $a = 0.1457$. $b = 1.5, \delta = 0.01, \alpha = \pi/2 - 0.08$.

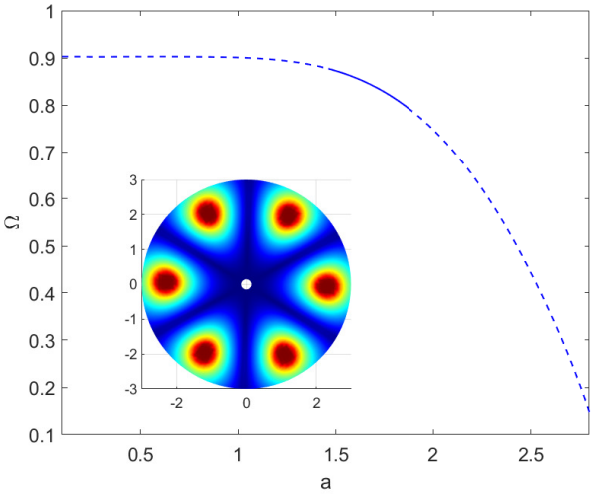

FIG. 7. Existence and stability of a six-head chimera. Ω is plotted as a function of a for the six-head chimera. Solid: stable; dashed: unstable. The inset shows $|z|$ for the unstable solution at $a = 0.14616$. $b = 3, \delta = 0.01, \alpha = \pi/2 - 0.08$.

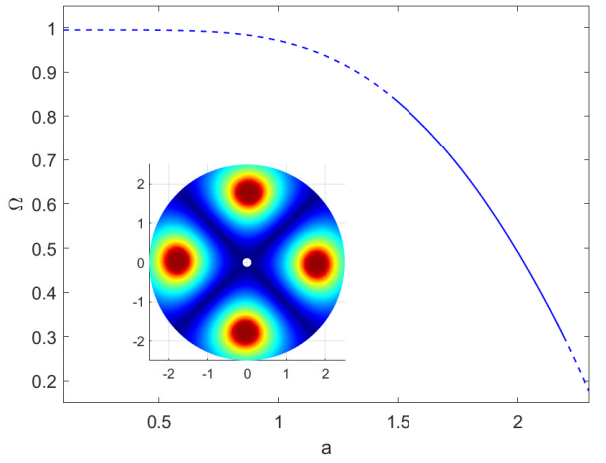

FIG. 6. Existence and stability of a four-head chimera. Ω is plotted as a function of a for the four-head chimera. Solid: stable; dashed: unstable. The inset shows $|z|$ for the unstable solution at $a = 0.11097$. $b = 2.5, \delta = 0.01, \alpha = \pi/2 - 0.08$.

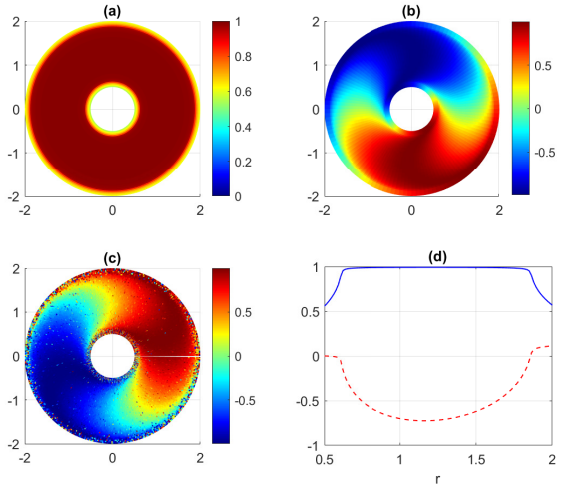

FIG. 8. An example of a rotating wave solution. (a): $|z|$ and (b): $\sin(\arg(z))$ for a solution of (4)-(5). (c): a snapshot of $\sin\theta$ for a solution of the discrete model (3). (d): $B_1(r)$ (solid blue) and $\Theta_1(r)$ (dashed red) corresponding to the steady state of (11). Parameters: $a = 0.5, b = 2, \delta = 0.01, \alpha = 1$.

V. ROTATING WAVES

For other initial conditions and parameter values it is possible to obtain rigidly rotating waves, with an example shown in Fig. 8. Panel (a) shows $|z|$ for a solution of (4)-(5). We see that is has dependence on r only and is close to 1 for most of the domain, corresponding to near synchrony, but decreases significantly at both the inner and outer boundaries, corresponding to asynchrony. Panel (b) shows $\sin(\arg(z))$ and we see that $\arg(z)$ varies by 2π during one rotation about the centre of the domain. Panel (c) shows $\sin\theta$ for a solution of the discrete network (3) for the same parameter values. The lower levels of synchrony near the inner and outer radii are clearly seen.

Such states have been considered previously in the limit of $a = 0$, for which there may be an incoherent "core" at the centre of a spiral wave, and these are referred to as "spiral wave chimeras"[30]. Similar spirals with incoherent cores have

been seen in other networks of nonlocally coupled oscillators on two-dimensional domains with a variety of domain shapes and coupling schemes[14,18,22,37,41,43,49,54]. Rotating waves of this form (but with phase locked oscillators) were studied in networks of identical oscillators in[10].

For rotating wave solutions of this form, we make the ansatz $z(r,\phi,t) = B_n(r,t)e^{i(-\Omega_n t + n\phi + \Theta_n(r,t))}$ where $n \in \mathbb{Z}$ is the winding number[8,10,30]. Then

$$\begin{aligned} R(r,\phi,t) &= \int_a^b s \int_{-\pi}^{\pi} W(r^2+s^2-2rs\cos\psi) z(s,\phi+\psi,t)\, d\psi\, ds \\ &= e^{-i\Omega_n t} \int_a^b s \int_{-\pi}^{\pi} W(r^2+s^2-2rs\cos\psi) B_n(s,t) e^{i(n(\phi+\psi)+\Theta_n(s,t))}\, d\psi \\ &= e^{-i\Omega_n t} e^{in\phi} e^{-r^2} \int_a^b B_n(s,t) s e^{-s^2} e^{i\Theta_n(s,t)} \int_{-\pi}^{\pi} e^{2rs\cos\psi} e^{in\psi}\, d\psi\, ds \\ &= 2\pi e^{-i\Omega_n t} e^{in\phi} e^{-r^2} \int_a^b B_n(s,t) I_n(2rs) s e^{-s^2} e^{i\Theta_n(s,t)} ds \\ &\equiv 2 e^{-i\Omega_n t} e^{in\phi} F_n(r) \end{aligned}$$

where I_n is the modified Bessel function of the first kind. Substituting this ansatz for z into (4) we obtain

$$\frac{\partial B_n}{\partial t} + iB_n \frac{\partial \Theta_n}{\partial t} = (i\Omega_n - \delta)B_n + e^{-i(\alpha+\Theta_n)} F_n - e^{i(\alpha+\Theta_n)} \bar{F}_n B_n^2, \tag{11}$$

the real and imaginary parts of which give the dynamics for the radially-dependent variables B_n and Θ_n, respectively. We are interested in steady states of (11), which correspond to waves like that in Fig. 8 which rigidly rotate about the origin with frequency Ω_n. (Note that if $n = 0$ we obtain the rotationally symmetric solutions studied in Sec. II.) Steady states of (11) are invariant under a uniform phase shift $\Theta_n(r) \to \Theta_n(r) + \gamma$ for any constant γ, so we set $\Theta_n(a) = 0$ to remove this invariance (see Fig. 8(d)). Setting $\delta = 0$ and $B_n = 1$, i.e. assuming identical oscillators which are phase locked, the steady state of (11) is equivalent to (2.5)-(2.6) in[10], which are expressions describing rotating waves for identical oscillators on an annulus.

A. Varying a

As a demonstration of the effects of varying the geometry we fix $b = 4$ and $\alpha = 0.3$ and vary a for different values of n. The results are shown in Fig. 9. We see that all solutions of this form are stable for a sufficiently close to b, i.e. for sufficiently narrow annuli, but they all lose stability as a is decreased, through apparently subcritical Hopf bifurcations. (Stability is determined by linearising the full dynamics around such solutions.) The values of a at which the rotating waves undergo bifurcations are $0.21793, 0.74186, 1.2688, 2.0523, 3.2752$, for $n = 1,2,3,4,5$, respectively. For all solutions, oscillators at the inner boundary become significantly asynchronous as a is decreased while the rest remain largely synchronised, i.e. the solutions approach spiral wave chimeras, although with different numbers of "arms" depending on the value of n. This phenomenon (the breakup of synchrony as a is decreased) was also observed by[10], who conjectured that these chimeras are created in a saddle-node-on-invariant-circle bifurcation.

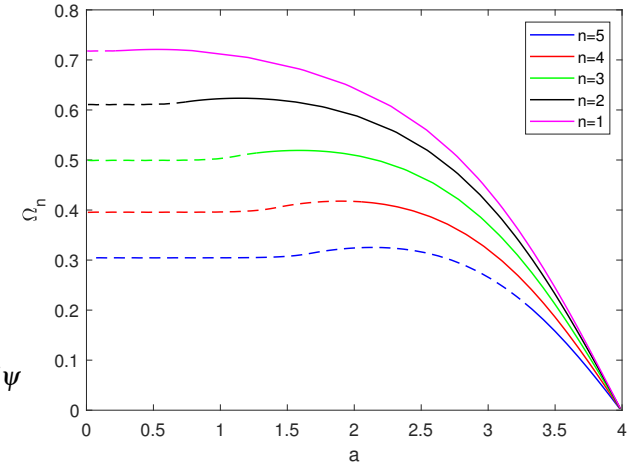

FIG. 9. Existence and stability of rotating waves for a fixed outer radius. Ω is plotted as a function of the inner radius a for rotating waves with different values of the winding number n. Solid: stable; dashed: unstable. Parameters: $b = 4, \delta = 0.01, \alpha = 0.3$.

In the limit $a \to b$ the domain becomes a ring, and these rotating waves approach the *twisted waves* studied in[35]. Their existence and stability, for a fixed coupling function, depends on parameters α and δ, as well as their winding number n.

B. Varying b

Alternatively, we fix $a = 2, \alpha = 0.3$ and vary b for different values of n. The results are shown in Fig. 10. The waves with $n = 1$ and 2 are stable over the range shown. The $n = 3$ wave is stable for $b = 2.48 < b$ while the $n = 4$ wave is stable only for the range $4.11 < b < 6.88$. All of the bifurcations shown are subcritical Hopf bifurcations. As with varying a, it seems that waves with smaller winding numbers n are stable over a wider range of parameters. For the parameters shown the oscillators remain essentially synchronised.

C. Varying α

We now fix $a = 1, b = 3$ and consider varying α. This parameter was varied in several previous papers investigating spiral wave chimeras[18,22,30,54], and it was found that Ω linearly increased with α before reaching a maximum and then decreasing. The spiral wave chimeras were stable either for α positive and less than some value[18,30,54], or over an interval bounded away from both zero and $\pi/2$[22]. Identified instabilities include Hopf[22] and symmetry-breaking[54].

In Fig. 11 we show the results of varying α for rotating waves on an annulus, for $n = 1,2,3,4$. As with spiral wave chimeras, Ω_n linearly increases with α before reaching a maximum and decreasing. For $n = 1,2$ the waves are stable for α

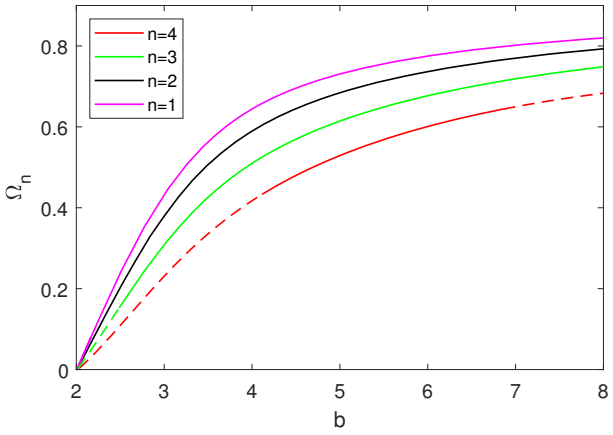

FIG. 10. Existence and stability of rotating waves for a fixed inner radius. Ω is plotted as a function of the outer radius b for rotating waves with different values of the winding number n. Solid: stable; dashed: unstable. Parameters: $a = 2, \delta = 0.01, \alpha = 0.3$.

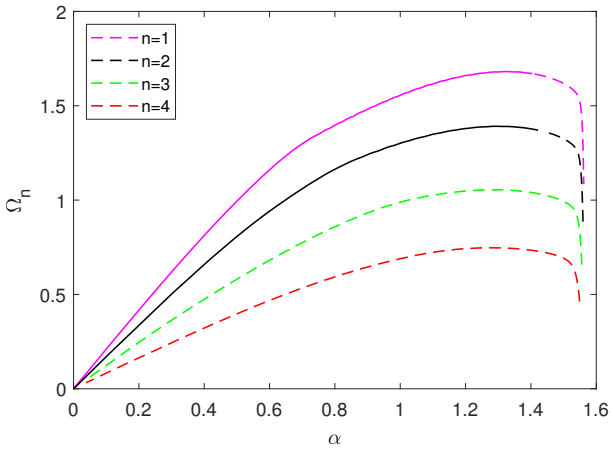

FIG. 11. Existence and stability of rotating waves as α is varied. Ω is plotted as a function of α for rotating waves with different values of the winding number n on a fixed domain. For $n = 1, 2$ the instability is through a Hopf bifurcation. Solid: stable; dashed: unstable. Parameters: $a = 1, b = 3, \delta = 0.01$.

less than particular values ($\alpha = 1.41$ for $n = 1$ and $\alpha = 1.44$ for $n = 2$) while the $n = 3, 4$ waves are always unstable. (They are stable steady states of (11) but are unstable steady states of (7).) The $n = 1, 2$ branches become unstable through subcritical Hopf bifurcations. For small α, the oscillators are essentially synchronised and $\Theta_n(r)$ is almost constant, i.e. contours of constant phase are close to just radial lines, as for solutions on a disc[30]. As α is increased oscillators at the inner and outer radii become asynchronous. Contours of constant phase become curved, as seen in Fig. 8(b) and (c). As α approaches $\pi/2$ the solutions collide with the zero solution, a steady state of (7), whose stability we analyse next.

VI. ZERO SOLUTION

$z = 0$ is a steady state of (4), and linearising (4) about this solution we have

$$\frac{\partial z(r,\phi,t)}{\partial t} = -\delta z + e^{-i\alpha} R/2 \tag{12}$$

where

$$R(r,\phi,t) = \int_a^b s \int_{-\pi}^{\pi} W(r^2 + s^2 - 2rs\cos\psi) z(s,\phi+\psi,t)\, d\psi\, ds \tag{13}$$

Since (12) is linear and we are looking for instabilities to rotating waves we assume a solution of the form $z(r,\phi,t) = e^{\lambda_m t} e^{im\phi} v_m(r)$ for $m \in \mathbb{Z}$. Using the Gaussian kernel (2) we have

$$R(r,\phi,t) = e^{\lambda_m t} e^{im\phi} e^{-r^2} \int_a^b s e^{-s^2} v_m(s) \int_{-\pi}^{\pi} e^{2rs\cos\psi} e^{im\psi}\, d\psi\, ds \tag{14}$$

$$= 2\pi e^{\lambda_m t} e^{im\phi} e^{-r^2} \int_a^b s e^{-s^2} v_m(s) I_m(2rs) ds \tag{15}$$

Substituting this and the assumed form of $z(r,\phi,t)$ into (12) we obtain

$$\lambda_m v_m(r) = -\delta v_m(r) + \pi e^{-i\alpha} [G v_m](r) \tag{16}$$

where

$$[G\eta](r) \equiv \int_a^b s e^{-s^2} e^{-r^2} I_m(2rs) \eta(s) ds \tag{17}$$

Discretising this integral converts (16) into a standard eigenvalue problem which we can solve numerically, for a range of values of m. The eigenvalues associated with the integral operator (17) are real and positive[1], so we see that for $\alpha = \pi/2$, all λ_m have real parts equal to $-\delta$, i.e. the origin is stable. Decreasing α from $\pi/2$ we find that eigenvalues move into the right half plane, with the right-most one for $m = 0$ going first, then the right-most one for $m = 1$ etc. The only possibility for having a stable solution branch off the origin is the $m = 0$ case, giving rotationally symetric solutions. This branch is shown in Fig. 12; it quickly becomes unstable through a symmetry-breaking bifurcation as α is decreased.

When eigenvalues cross into the right half plane their imaginary part is just Ω, the speed at which we must rotate the coordinate frame to keep the solutions created in these bifurcations stationary. Even though the only meaningful values of m are the integers, we can treat m as a continuous variable and follow the path in the (m,α) plane along which the rightmost λ_m lies on the imaginary axis. Plotting Ω as a function of α along this path we obtain the dotted black curve in Fig. 12, where the points corresponding to integer values of m are shown with stars. (The dotted black curve does not continue to the right of the $m = 0$ point, as the origin is stable there.) Also shown in Fig. 12 is Ω for the rotationally symmetric solution ($m = 0$) and the curves already shown in Fig. 11 (now using m instead of n) and we see that these rotating waves are indeed created in bifurcations from the origin.

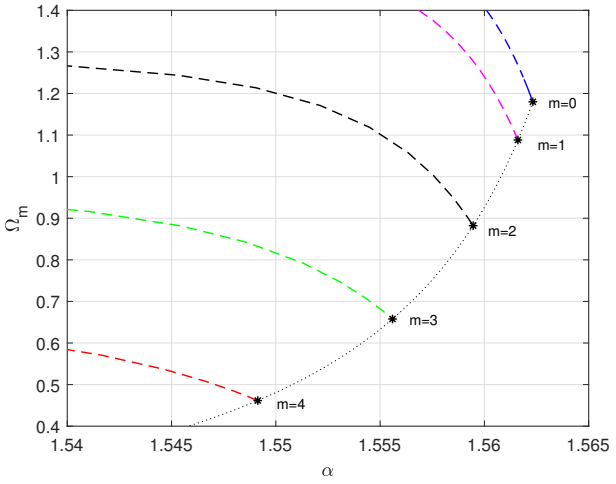

FIG. 12. Bifurcations from the zero solution. Coloured curves: Ω as a function of α for rotating waves with different values of n (or m). All but the $m=0$ curve are also plotted in Fig. 11. All rotating wave solutions shown are unstable apart from those on the $m=0$ branch (describing rotationally symmetric solutions) for $1.18<\Omega_0<1.24$. The dotted black curve is explained in the text. Parameters: $a=1, b=3, \delta=0.01$.

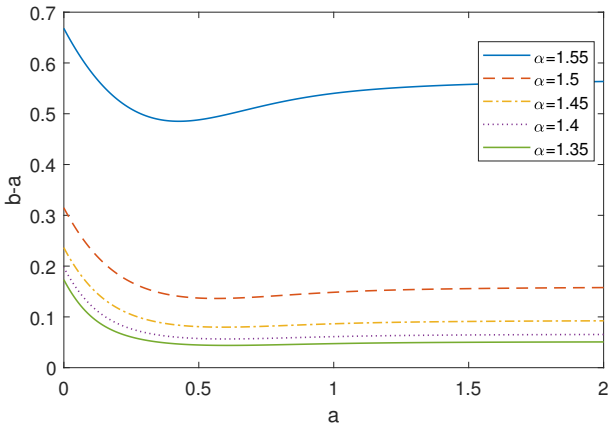

FIG. 13. Regions of stability of the origin as a (inner radius) and $b-a$ (width of the annulus) are varied for various values of α. For a given value of α, the origin is stable below the curve. Instability is calculated for the $m=0$ mode. Parameter: $\delta=0.01$.

To further understand the stability of the origin we assume that is becomes unstable via the $m=0$ mode and follow this instability (a purely imaginary eigenvalue) as both a (the inner radius) and $b-a$ (the width of the annulus) are varied, for several values of α close to $\pi/2$. The results are shown in Fig 13. We see that only for narrow annuli is the origin stable, and it goes unstable as either the width is increased, or α is decreased.

Note that the stability of the origin for a range of parameter values is a result of having $\delta\neq 0$, i.e. heterogeneous oscillators. If $\delta=0$ we see from (16) that when $\alpha=\pi/2$ the λ_m are all purely imaginary, and as soon as α is decreased, they all have positive real part, i.e. the origin is unstable. This is another example of heterogeneity "unfolding" the degenerate dynamics which occur for identical oscillators[17].

VII. DISCUSSION

We have studied various spatiotemporal patterns that occur in a network of nonlocally coupled heterogeneous phase oscillators on an annular domain. Using the Ott/Antonsen ansatz we derived a continuum level description of the dynamics in terms of the local order parameter $z(\mathbf{x},t)\in\mathbb{C}$. Due to the heterogeneity oscillators are never exactly synchronised, but differing levels of synchrony in different parts of the domain correspond to differing values of $|z(\mathbf{x},t)|$, where the dynamics of z are given by (4)-(5). Some of the patterns seen can be classified as chimeras, while for others the varying levels of synchrony are just a result of the domain used. We used a Gaussian coupling kernel, which allowed some integrals to be evaluated analytically.

We first considered rotationally symmetric patterns and then moved to multi-headed chimeras, which are analogous to those seen on ring domains[29]. We then considered rotating waves, analogous to those studied in[10], a special case of which corresponds to a spiral wave chimera[30]. Through numerical bifurcation analysis we determined ranges of parameters for which various solutions are stable, and the bifurcations in which they lose stability. Interestingly, all bifurcations were found to be subcritical. We did follow the multi-headed chimeras shown in Sec. IV as α was varied and found curves similar in shape to those in Fig. 11 (i.e. solutions persist down to $\alpha=0$); however, these solutions become unstable as α is decreased (not shown). Thus in keeping with previous results[37], chimeras appear to be stable only for α slightly less than $\pi/2$[3], while rotating waves, like spiral wave chimeras, are only stable for small α[30]. The reasons for this remain unclear.

Our analysis is not complete, since even keeping the level of heterogeneity (δ) fixed, there are three parameters of interest: the inner and outer radii, and the phase shift α. While we only discussed spatiotemporal patterns with regular structure, irregular patterns also exist, and an example is shown in Fig. 14 for both the continuum equations and the discrete network. The results presented here broaden our understanding of the possible dynamics of networks of coupled oscillators.

We now discuss possible further work. Networks of theta neurons have the same mathematical form as networks of sinusoidally coupled phase oscillators, so are also amenable to the use of the Ott/Antonsen ansatz, resulting in equations with a similar structure to (4)-(5)[6,19,34]. While these resulting neural field equations have been considered in one[11,19,21,24] and two[6,7] spatial dimensions, we are not aware of any studies on annular domains. Such studies would complement earlier ones which studied classical neural field equations, often with a Heaviside nonlinearity, on two-dimensional domains[9,25,40,48], and it would be interesting to see if any new phenomena occur in these "next generation" neural field models. Preliminary studies of such equations with a Mexican-hat

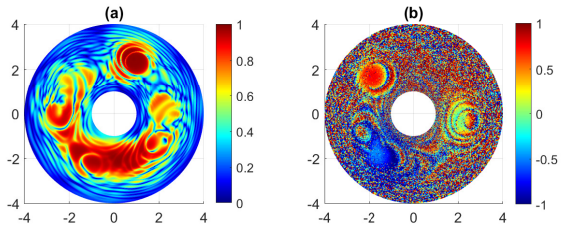

FIG. 14. Snapshots showing examples of complex behaviour. (a): $|z|$ from solving (4). (b): $\sin\theta$ from solving the discrete model (3). Parameters: $a = 1, b = 4, \alpha = 1.5, \delta = 0.01$.

coupling function show the existence of solutions like those in Fig. 4, but with isolated "bumps" of active neurons rather than regions of high synchrony (results not shown).

Author Declarations: The authors have no conflicts to disclose.

Acknowledgements: I thank Oleh Omel'chenko for discussions regarding the eigenvalues of the operator (17), and the referees for their helpful comments.

[1]Personal communication, Oleh Omel'chenko, 2022.
[2]Daniel M. Abrams, Rennie Mirollo, Steven H. Strogatz, and Daniel A. Wiley. Solvable model for chimera states of coupled oscillators. *Phys. Rev. Lett.*, 101:084103, 2008.
[3]Daniel M. Abrams and Steven H. Strogatz. Chimera states for coupled oscillators. *Phys. Rev. Lett.*, 93:174102, 2004.
[4]Daniel M. Abrams and Steven H. Strogatz. Chimera states in a ring of nonlocally coupled oscillators. *Int. J. Bifn. Chaos*, 16:21–37, 2006.
[5]J.A. Acebrón, LL Bonilla, C.J. Pérez Vicente, F. Ritort, and R. Spigler. The Kuramoto model: A simple paradigm for synchronization phenomena. *Rev. Mod. Phys.*, 77:137–185, 2005.
[6]Áine Byrne, Reuben D O'Dea, Michael Forrester, James Ross, and Stephen Coombes. Next-generation neural mass and field modeling. *Journal of neurophysiology*, 123(2):726–742, 2020.
[7]Áine Byrne, James Ross, Rachel Nicks, and Stephen Coombes. Mean-field models for eeg/meg: from oscillations to waves. *Brain topography*, 35(1):36–53, 2022.
[8]Donald S Cohen, John C Neu, and Rodolfo R Rosales. Rotating spiral wave solutions of reaction-diffusion equations. *SIAM journal on applied mathematics*, 35(3):536–547, 1978.
[9]Stephen Coombes, Helmut Schmidt, and Ingo Bojak. Interface dynamics in planar neural field models. *The Journal of Mathematical Neuroscience*, 2(1):1–27, 2012.
[10]B. Ermentrout and Y. Ding. Rotating waves of nonlocally coupled oscillators on an annulus, 2022. submitted.
[11]Jose M Esnaola-Acebes, Alex Roxin, Daniele Avitabile, and Ernest Montbrió. Synchrony-induced modes of oscillation of a neural field model. *Physical Review E*, 96(5):052407, 2017.
[12]Vladimir García-Morales and Katharina Krischer. The complex ginzburg–landau equation: an introduction. *Contemporary Physics*, 53(2):79–95, 2012.
[13]Sindre W Haugland. The changing notion of chimera states, a critical review. *Journal of Physics: Complexity*, 2021.
[14]P.J. Kim, T.W. Ko, H. Jeong, and H.T. Moon. Pattern formation in a two-dimensional array of oscillators with phase-shifted coupling. *Physical Review E*, 70(6):065201, 2004.
[15]Y. Kuramoto and D. Battogtokh. Coexistence of Coherence and Incoherence in Nonlocally Coupled Phase Oscillators. *Nonlinear Phenom. Complex Syst.*, 5:380–385, 2002.
[16]Yoshiki. Kuramoto. *Chemical oscillations, waves, and turbulence*. Springer-Verlag, 1984.
[17]Carlo R. Laing. Chimera states in heterogeneous networks. *Chaos*, 19:013113, 2009.
[18]Carlo R Laing. The dynamics of chimera states in heterogeneous kuramoto networks. *Physica D: Nonlinear Phenomena*, 238(16):1569–1588, 2009.
[19]Carlo R Laing. Derivation of a neural field model from a network of theta neurons. *Physical Review E*, 90(1):010901, 2014.
[20]Carlo R Laing. Chimeras in networks with purely local coupling. *Physical Review E*, 92(5):050904, 2015.
[21]Carlo R Laing. Exact neural fields incorporating gap junctions. *SIAM Journal on Applied Dynamical Systems*, 14(4):1899–1929, 2015.
[22]Carlo R Laing. Chimeras in two-dimensional domains: heterogeneity and the continuum limit. *SIAM Journal on Applied Dynamical Systems*, 16(2):974–1014, 2017.
[23]Carlo R Laing. Dynamics and stability of chimera states in two coupled populations of oscillators. *Physical Review E*, 100(4):042211, 2019.
[24]Carlo R Laing and Oleh Omel'chenko. Moving bumps in theta neuron networks. *Chaos: An Interdisciplinary Journal of Nonlinear Science*, 30(4):043117, 2020.
[25]Carlo R Laing and William C Troy. Pde methods for nonlocal models. *SIAM Journal on Applied Dynamical Systems*, 2(3):487–516, 2003.
[26]Hon Wai Lau and Jörn Davidsen. Linked and knotted chimera filaments in oscillatory systems. *Physical Review E*, 94(1):010204, 2016.
[27]Volodymyr Maistrenko, Oleksandr Sudakov, Oleksiy Osiv, and Yuri Maistrenko. Multiple scroll wave chimera states. *The European Physical Journal Special Topics*, 226(9):1867–1881, 2017.
[28]Yuri Maistrenko, Oleksandr Sudakov, Oleksiy Osiv, and Volodymyr Maistrenko. Chimera states in three dimensions. *New Journal of Physics*, 17(7):073037, 2015.
[29]Yuri L Maistrenko, Anna Vasylenko, Oleksandr Sudakov, Roman Levchenko, and Volodymyr L Maistrenko. Cascades of multiheaded chimera states for coupled phase oscillators. *International Journal of Bifurcation and Chaos*, 24(08):1440014, 2014.
[30]Erik A Martens, Carlo R Laing, and Steven H Strogatz. Solvable model of spiral wave chimeras. *Physical review letters*, 104(4):044101, 2010.
[31]O E Omel'chenko. The mathematics behind chimera states. *Nonlinearity*, 31(5):R121–R164, apr 2018.
[32]OE Omel'chenko. Mathematical framework for breathing chimera states. *Journal of Nonlinear Science*, 32(2):1–34, 2022.
[33]Oleh Omel'chenko. Periodic orbits in the ott-antonsen manifold. *arXiv preprint arXiv:2206.01481*, 2022.
[34]Oleh Omel'chenko and Carlo R Laing. Collective states in a ring network of theta neurons. *Proceedings of the Royal Society A*, 478(2259):20210817, 2022.
[35]Oleh Omel'chenko, Matthias Wolfrum, and Carlo R Laing. Partially coherent twisted states in arrays of coupled phase oscillators. *Chaos: An Interdisciplinary Journal of Nonlinear Science*, 24(2):023102, 2014.
[36]Oleh E Omel'chenko. Coherence–incoherence patterns in a ring of nonlocally coupled phase oscillators. *Nonlinearity*, 26(9):2469, 2013.
[37]Oleh E Omel'chenko, Matthias Wolfrum, Serhiy Yanchuk, Yuri L Maistrenko, and Oleksandr Sudakov. Stationary patterns of coherence and incoherence in two-dimensional arrays of non-locally-coupled phase oscillators. *Physical Review E*, 85(3):036210, 2012.
[38]Edward Ott and Thomas M. Antonsen. Low dimensional behavior of large systems of globally coupled oscillators. *Chaos*, 18:037113, 2008.
[39]Edward Ott and Thomas M Antonsen. Long time evolution of phase oscillator systems. *Chaos: An interdisciplinary journal of nonlinear science*, 19(2):023117, 2009.
[40]Markus R Owen, Carlo R Laing, and Stephen Coombes. Bumps and rings in a two-dimensional neural field: splitting and rotational instabilities. *New Journal of Physics*, 9(10):378, 2007.
[41]Mark J Panaggio and Daniel M Abrams. Chimera states on a flat torus. *Physical review letters*, 110(9):094102, 2013.
[42]Mark J Panaggio and Daniel M Abrams. Chimera states: coexistence of coherence and incoherence in networks of coupled oscillators. *Nonlinearity*, 28(3):R67, 2015.
[43]Mark J Panaggio and Daniel M Abrams. Chimera states on the surface of a sphere. *Physical Review E*, 91(2):022909, 2015.
[44]Mark J Panaggio, Daniel M Abrams, Peter Ashwin, and Carlo R Laing. Chimera states in networks of phase oscillators: the case of two small populations. *Physical Review E*, 93(1):012218, 2016.

[45] Diego Pazó and Ernest Montbrió. Low-dimensional dynamics of populations of pulse-coupled oscillators. *Physical Review X*, 4(1):011009, 2014.
[46] A. Pikovsky, M. Rosenblum, and J. Kurths. *Synchronization*. Cambridge University Press, 2001.
[47] Arkady Pikovsky and Michael Rosenblum. Partially integrable dynamics of hierarchical populations of coupled oscillators. *Phys. Rev. Lett.*, 101:264103, 2008.
[48] James Rankin, Daniele Avitabile, Javier Baladron, Gregory Faye, and David JB Lloyd. Continuation of localized coherent structures in nonlocal neural field equations. *SIAM Journal on Scientific Computing*, 36(1):B70–B93, 2014.
[49] S. Shima and Y. Kuramoto. Rotating spiral waves with phase-randomized core in nonlocally coupled oscillators. *Physical Review E*, 69(3):036213, 2004.
[50] S.H. Strogatz. From Kuramoto to Crawford: exploring the onset of synchronization in populations of coupled oscillators. *Physica D*, 143:1–20, 2000.
[51] S. Watanabe and SH Strogatz. Constants of motion for superconducting Josephson arrays. *Physica. D*, 74:197–253, 1994.
[52] Matthias Wolfrum and O Omel'chenko. Chimera states are chaotic transients. *Physical Review E*, 84(1):015201, 2011.
[53] Matthias Wolfrum, Oleh E Omel'chenko, Serhiy Yanchuk, and Yuri L Maistrenko. Spectral properties of chimera states. *Chaos: An Interdisciplinary Journal of Nonlinear Science*, 21(1):013112, 2011.
[54] Jianbo Xie, Edgar Knobloch, and Hsien-Ching Kao. Twisted chimera states and multicore spiral chimera states on a two-dimensional torus. *Physical Review E*, 92(4):042921, 2015.
[55] Anna Zakharova. *Chimera Patterns in Networks*. Springer, 2020.